3-7-2019

Computationally Efficient Strand Eddy Current Loss Calculation in Electric Machines

Alireza Fatemi
General Motors Company

Dan M. Ionel
University of Kentucky

Nabeel Demerdash
Marquette University, nabeel.demerdash@marquette.edu

Dave A. Staton
Motor Design, Ltd.

Rafal Wrobel
Newcastle University

See next page for additional authors

Accepted version. *IEEE Transactions on Industry Applications*, Vol. 55, No. 4 (July/August 2019): 3479 - 3489. DOI.

Computationally Efficient Strand Eddy Current Loss Calculation in Electric Machines

Alireza Fatemi
Global Research and Development Department, Warren Technical Center, General Motors Company, Warren, MI, USA

Dan M. Ionel
Department of Electrical and Computer Engineering, University of Kentucky, Lexington, KY, USA

Nabeel A. O. Demerdash
Department of Electrical and Computer Engineering, Marquette University, Milwaukee, WI, USA

Dave A. Staton
Motor Design Ltd., Ellesmere, U.K.

Rafal Wrobel
Newcastle University, Newcastle upon Tyne, U.K.

Yew Chuan Chong

Motor Design Ltd., Ellesmere, U.K.

Abstract:

A fast finite element (FE) based method for the calculation of eddy current losses in the stator windings of randomly wound electric machines is presented in this paper. The method is particularly suitable for implementation in large-scale design optimization algorithms where a qualitative characterization of such losses at higher speeds is most beneficial for identification of the design solutions that exhibit the lowest overall losses including the ac losses in the stator windings. Unlike the common practice of assuming a constant slot fill factor s_f for all the design variations, the maximum s_f in the developed method is determined based on the individual slot structure/dimensions and strand wire specifications. Furthermore, in lieu of detailed modeling of the conductor strands in the initial FE model, which significantly adds to the complexity of the problem, an alternative rectangular coil modeling subject to a subsequent flux mapping technique for determination of the impinging flux on each individual strand is pursued. Rather than pursuing the precise estimation of ac conductor losses, the research focus of this paper is placed on the development of a computationally efficient technique for the derivation of strand eddy current losses applicable in design optimization, especially where both the electromagnetic and thermal machine behavior are accounted for. A fractional-slot concentrated winding permanent magnet synchronous machine is used for the purpose of this study due to the higher slot leakage flux and slot opening fringing flux of such machines, which are the major contributors to strand eddy current losses in the windings. The analysis is supplemented with an investigation on the influence of the electrical loading on ac winding loss effects for this machine design, a subject that has received less attention in the literature. Experimental ac loss measurements on a 12-slot 10-pole stator assembly will be discussed to verify the existing trends in the simulation results.

SECTION I. Introduction

The eddy current effects including the skin, strand-level, and bundle-level proximity effects [1] potentially constitute a significant contributor to the overall copper losses in the stator windings of high-speed permanent magnet (PM) machines. Even if preventive measures such as stranding and transposition are adopted, the ac conductor losses in the stator windings of PM motors can still be significant for high power density high speed open-slot fractional-slot concentrated winding (FSCW) machines due to the prevalence of slot leakage flux, and slot opening fringing flux, e.g., see Fig. 1. Common techniques for the estimation of such losses are especially prohibitive for randomly wound coil configurations and require a significant amount of time to formulate and solve the ac electromagnetic (EM) problem at the conductor strand level. The development of a high-fidelity loss characterization method to provide a basis of qualitative ac loss comparison between thousands of design candidates, which is suitable for implementation in large-scale design optimization algorithms, is imperative. In addition to the value of the ac loss, the distribution of the overall copper losses in the stator winding is of interest particularly if coupled thermal–EM design optimization is desired [2], [3].

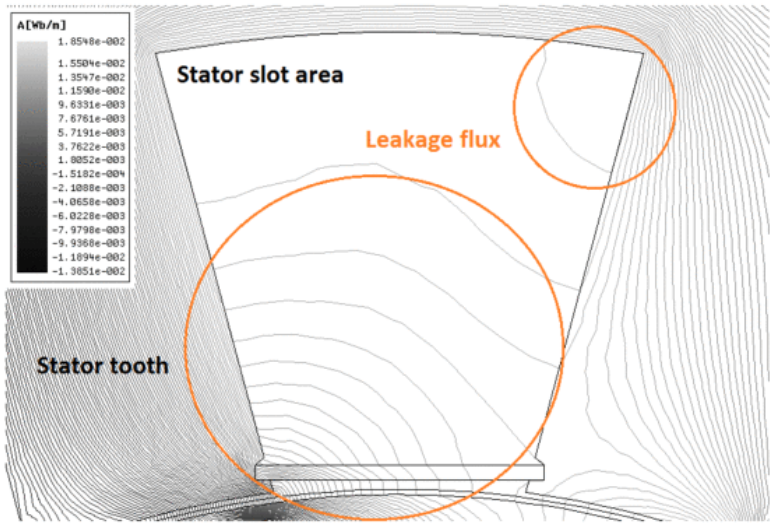

Fig. 1. Slot leakage and fringing flux in a typical FSCW PM machine.

In a broad categorization, the popular methods for analysis of eddy current losses in PM machines rely on analytical models as in [4]–[5][6][7][8][9][10][11][12], numerical finite element (FE)/difference analysis as in [13]–[14][15][16], or rely on combined analytical-FE-experimental procedures as in [17]–[18][19]. The analytical models lack the desired accuracy under magnetic core saturation and are not applicable to complex geometry without further compromising the accuracy. The numerical models are not suitable for integration into large-scale design optimization processes due to time-consuming computations. The combined procedures require extensive *a priori* experimentations and are best suited for comparative loss analysis between different motor technologies and winding configurations as opposed to application for large-scale design optimization of one particular configuration.

In this paper, an FE-based modeling technique is presented for estimation of the strand eddy current losses in the stator windings of electric machines, with an emphasis on sinusoidally excited PM synchronous machines. This is in order to include the portion of the ac losses that stems from the presence of slot leakage and fringing fluxes in the performance characterization of such machines. The developed hybrid analytical–numerical loss calculation method is rendered computationally efficient (CE) through adopting several measures, such as alternative coil modeling, which reduces the computation time required for solving the FE model, exploiting the existing electric symmetry in addition to the magnetic periodicity of PM machines with sinusoidal current excitation, and implementing fast analytical techniques for mapping the flux within the slot area, estimating the fill factor and strand locations, and finally characterization of the eddy current losses based on the value of the flux density impinging on each stator winding conductor [20]. The presented loss calculation method does not account for ac losses that are three-dimensional (3-D) in nature [21]; thus, the effects of twisting and transposition throughout the length of the conductors are not considered, neither does it address the circulating losses appearing in bundled conductors [17], [22], as these losses do not occur at the strand level. However, the presented method accounts for the effects of motion, saturation, and interaction between stator and rotor magnetomotive forces, and provides a reasonable compromise between computational time and accuracy, which makes it suitable for application in the large-scale design optimization of PM machines in the initial stages of the design. Examples of such large-scale design optimization algorithms in which thousands of design candidates with several control parameters are evaluated are reported in [23]–[24][25][26][27][28].

Using the developed method, strand eddy current losses under various loading conditions are computed and the existing trends between the ratio of ac to dc losses, $P_{\mathrm{ac}}/P_{\mathrm{dc}}$, with respect to the loading level are studied. Through this analysis, it is demonstrated that the traditional figure of merit for comparison of ac losses in

electric machines, which is established by the ratio of ac to dc resistance, $R_{\mathrm{ac}}/R_{\mathrm{dc}}$, is by definition incapable of modeling the effects of the loading level on the ratio of $P_{\mathrm{ac}}/P_{\mathrm{dc}}$.

This paper is organized as follows. Section II provides a brief review example of previous studies on characterization of the eddy current losses in electric machines. The proposed method of eddy current loss calculation is described step by step in Section III, and is further discussed through a case-study analysis in Section IV. Finally, Section V is dedicated to conclusions and future work.

SECTION II. Strand Eddy Current Loss Characterization

Analytical models for the calculation of eddy current losses in electric machines are reported for 1-D single-slot models as in [8], 2-D single-slot models as in [9], or 2-D machine models as in [10]. These methods provide an insight into the nature of the eddy current losses but do not accurately account for the non-linearity of the magnetic core, and are difficult to apply to complex machine geometries.

Numerical models require a significantly large number of elements in the stator slots and are therefore time-consuming to solve. In some studies with detailed coil models [13], [15], a uniform distribution of current is assumed in the conductors so that a time-stepping magnetostatic solution, i.e., magnetostatic solutions at different rotor positions, can be performed. Subsequently, a detailed distribution of the radial and tangential components of flux density $B_{R,T}$in each stator slot is obtained by establishing a fine grid over each slot pitch of the stator from one tooth axis to the next. These values are used in a numerical harmonic analysis expressed by

$$B_{R,T}(t) = \sum_{k=1}^{\infty} |B_{2k-1,(R,T)}| \sin((2k-1)\omega t - \phi_{2k-1,(R,T)}) \qquad (1)$$

where ω is the fundamental frequency of the rotating magnetic field.

Accordingly, the eddy current loss P_e in watts per strand per depth of axial length, for a rectangular copper strand of width a and height b subject to a uniform time-varying flux density of (1), can be obtained using

$$P_e = ab \sum_{k=1}^{\infty} \frac{(2k-1)^2\omega^2}{24\rho} (|B_{2k-1,R}|^2 a^2 + |B_{2k-1,T}|^2 b^2) \times \eta_{2k-1} \qquad (2)$$

where the skin effect coefficient η_{2k-1} is given by [29]

$$\eta_{2k-1} = \frac{3}{4\alpha_{2k-1}^2} \frac{\sinh(2\alpha_{2k-1}) - \sin(2\alpha_{2k-1})}{\cosh(2\alpha_{2k-1}) - \cos(2\alpha_{2k-1})}$$
$$\alpha_{2k-1} = \frac{a}{6320} \sqrt{\frac{\mu_r (2k-1) f}{\rho}}. \qquad (3)$$

In the case of round conductors of diameter d and resistivity ρ, (1) can be used for calculating the magnitude of the impinging flux $|B_{2k-1}| = \sqrt{|B_{2k-1,R}|^2 + |B_{2k-1,T}|^2}$, with the eddy current loss per depth of axial length given by [1]

$$P_e = \pi d^4 \sum_{k=1}^{\infty} \frac{(2k-1)\omega^2 |B_{2k-1}|^2}{128\rho}. \qquad (4)$$

The ratio of ac to dc resistance r_{ac} of round conductors can be modified according to (5)in order to also include the skin effect [1]

$$r_{\mathrm{ac}} = \frac{d}{8\delta}\mathrm{Re}\left((1+j)\frac{I_0\left(\frac{d}{2\delta}(1+j)\right)}{I_1\left(\frac{d}{2\delta}(1+j)\right)}\right), \delta = \sqrt{\frac{2\rho}{\omega\mu}} \qquad (5)$$

where I_0 and I_1 are Bessel functions of zero and first orders, respectively, and δ is the skin depth. The solution of r_{ac} for round conductors is documented through charts and graphs in [1], and can be readily found for a given conductor diameter and excitation frequency.

SECTION III. FE-Based Eddy Current Loss Estimation for Randomly Wound Stator Windings

For a given machine configuration, the distribution of the leakage/fringing flux within any slot is dependent on the following:

1. dimensions of the cross section;
2. the loading level;
3. the location of the conductors within the stator slots;
4. the temperatures of components;
5. the frequency of operation.

Only a thermally coupled time-stepping transient FE model with detailed knowledge of conductor locations can account for all the aforementioned parameters. The formulation and solution of such an EM problem is an extensively and computationally demanding process, not suitable for early design stage optimization purposes.

In this section, an alternative method will be presented. The steps of this CE loss calculation method, which can be integrated into a large-scale design optimization process, are described in the following section.

A. Modeling of the Coils

Detailed modeling of the coils in the slots, such as the one shown in Fig. 2(a), adds to the complexity of the FE model, and thus increases the computation time to reach a solution. As opposed to the crude coil model commonly used for EM-FE analysis, as shown in Fig. 2(b), here an alternative representation is developed. According to Fig. 2(c) and (d), the winding is divided into a number of rectangular areas over its radial and tangential dimensions.

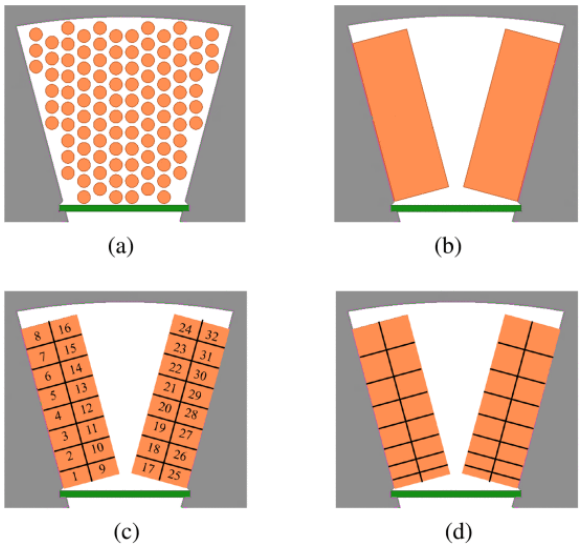

Fig. 2. Coil models for FE analysis of a typical electric machine. (a) Detailed model. (b) Common model. (c) Alternative model with identical sections. (d) Alternative model with skewed sections.

The heights and the widths of the sections can be all equal as in Fig. 2(c) or skewed as in Fig. 2(d) to provide more details at the slot opening. The radial and tangential components of the flux densities at the middle of each rectangular section can then be extracted. The sampled B profiles are subsequently used to map the flux density at any point in the slot. The minimum number of sections in each direction of the 2-D slot plane depends on the mapping method implemented for reconstruction of the flux density surface over the winding area in the stator slot. For example, if a polynomial surface fit is used, the number of samples should be chosen according to the order of the polynomial equation representing the surface. Here, 32 sections with equal heights and equal widths are defined, as shown in Fig. 2(c), to be used with the mapping method described in Section III-D.

B. Extraction of B Field Profiles Inside the Slot

The value of B at the middle of each section can be obtained by any time-stepping magnetostatic FE analysis including the CE-FEA method [30]. The CE-FEA method exploits the electric symmetry in the stator windings of sine wave operated/energized PM motors to reconstruct the profile of the flux density waveforms over the full electrical cycle by performing FEA over a window of 60 electrical degree. The CE-FEA method was developed and compared with the detailed time-stepping transient FEA (TS-FEA) in [30]. Subsequently, it was used in large-scale design optimizations of PM machines in [23] and [26]–[28], and also was utilized in calculation of eddy current PM losses in concentrated winding PM machines in [31].

Here, the CE-FEA method is used to extract the radial and tangential components of the sampled B profiles for the coil pieces shown in Fig. 2(c) for a typical machine under full-load motoring operation with counterclockwise (CCW) rotation. The B profiles for selected sections are shown in Fig. 3(a)–(d). It is interesting to note that the major component of the slot leakage flux is tangential. Furthermore, the decreasing trend of this slot leakage flux from top to bottom of the slot, and from left to right for the motoring operation, should be noted.

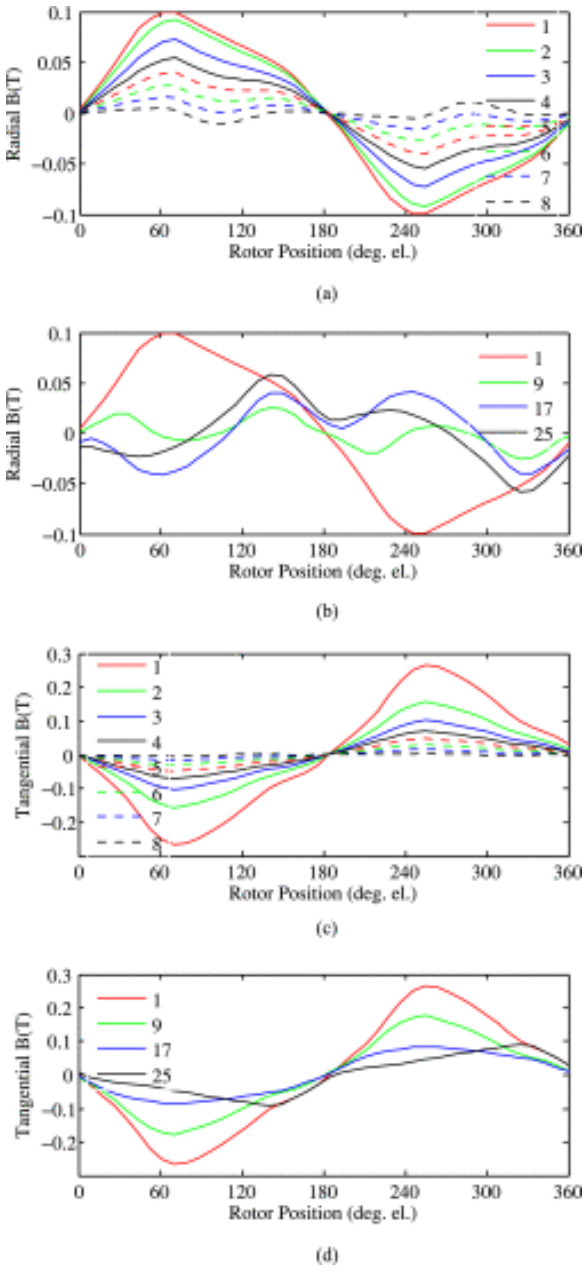

Fig. 3. Radial and tangential components of the field sections in Fig. 2(c) for a typical motor under full load. (a) Radial component of B moving into the slot. (b) Radial component of B moving along the slot opening. (c) Tangential component of B moving into the slot. (d) Tangential component of B moving along the slot opening.

C. Determination of the Slot Fill Factor and the Associated Conductor Positions

The slot fill factor s_f is defined as follows:

$$s_f = \frac{A_{\text{Cu}}}{A_{\text{slot}}} = \frac{n_C \pi d^2}{4A_{\text{slot}}} \qquad (6)$$

where A_{Cu} is the copper area within the slot area A_{slot}, and n_C is the number of conductors. In a large-scale design optimization problem, the slot dimensions and area vary between the design candidates. Accordingly, the maximum slot fill factor $s_{f,max}$ and the location of the conductors vary between the design candidates and

should be calculated for each individual design. Here, the $s_{f,max}$ is needed for the FEA to accurately account for the available ampere turn flowing through the alternate coil model described in the previous section. Furthermore, the conductor positions inside the slot are required for determining the impinging field on each strand in a post-FEA process using the B samples from FEA. This mapping process will be described in a later section.

Algorithm 1: Algorithm for calculation of fill factor and wire strand locations.

Input: slot dimensions, wire and insulation specifications

Output: $s_{f,max}$, strand locations

Initialization:

Create slot geometry and wire grid

LOOP Process

for $i = 1$ to i_{max} **do**

Move the slot over the wire grid by a random number

Identify the location and number of wire strands fitting inside the slot

Calculate s_f

if ($s_f > s_{f,max}$) **then**

$s_{f,max} = s_f$

Store new strand locations

end if

end for

return

The method that was implemented here for the calculation of $s_{f,max}$ and the associated positions of the conductors within the slot, which yields such $s_{f,max}$, relies on an optimization approach that is based on random perturbation of the slot geometry [32]. As described in the following and illustrated in Fig. 4, a given slot geometry including slot insulation is randomly moved with respect to a grid of tightly packed circular conductors, the diameter of which corresponds to the gauge and enamel of the wire. The fill factor is then compared for various slot perturbations and strand arrangements to determine the $s_{f,max}$ and the associated locationsof the strands.

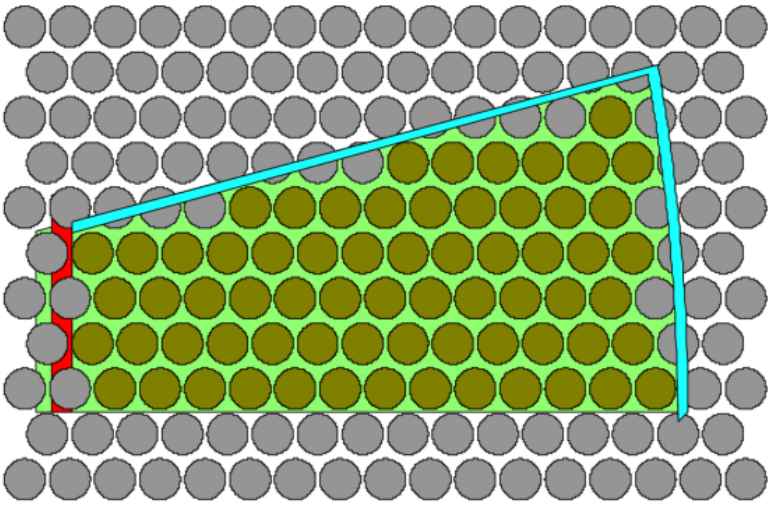

Fig. 4. Determination of $s_{f,max}$ and conductor positions by moving the slot geometry over a grid of conductors.

This method is used for the determination of $s_{f,max}$, for example, slot geometries shown in Fig. 5(a)–(c). As can be seen in this illustration, for a given conductor diameter, the achievable $s_{f,max}$ diminishes as the slot area decreases, which is successfully predicted by the method implemented here.

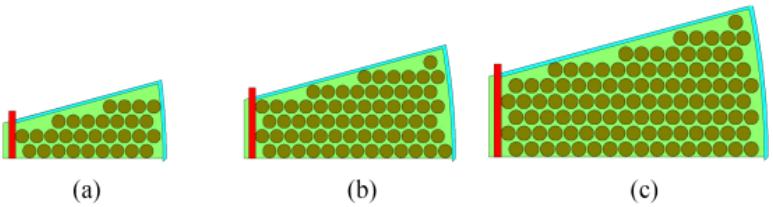

Fig. 5. Slot fill factor and strand positions, for example, slot geometries as the net slot area increases. (a) $s_{f,max} = 0.47$. (b) $s_{f,max} = 0.51$. (c) $s_{f,max} = 0.53$.

It should be pointed out that the assumption of maximum copper fill factor for any given slot dimension reduces the strand twist and transposition, and thus the variation of the impinging field across the length of the conductor.

D. Mapping the Flux on Each Individual Strand

When the B profiles over the full fundamental cycle are obtained for each rectangular coil section, the radial and tangential components are separately used in a time harmonic analysis according to (1). Subsequently, for each harmonic, a Delaunay triangulation method is implemented in MATLAB for interpolating the samples scattered over the slot at the points where the center of each strand conductor is located. This process is illustrated in Fig. 6 for the reconstruction surfaces of the first harmonic of the B field throughout the slot area. It should be noted that since the gap between the sampling points in the middle of the slot narrows toward the top of the slot where the leakage fields are stronger, the sampling resolution is desirably higher where it is needed.

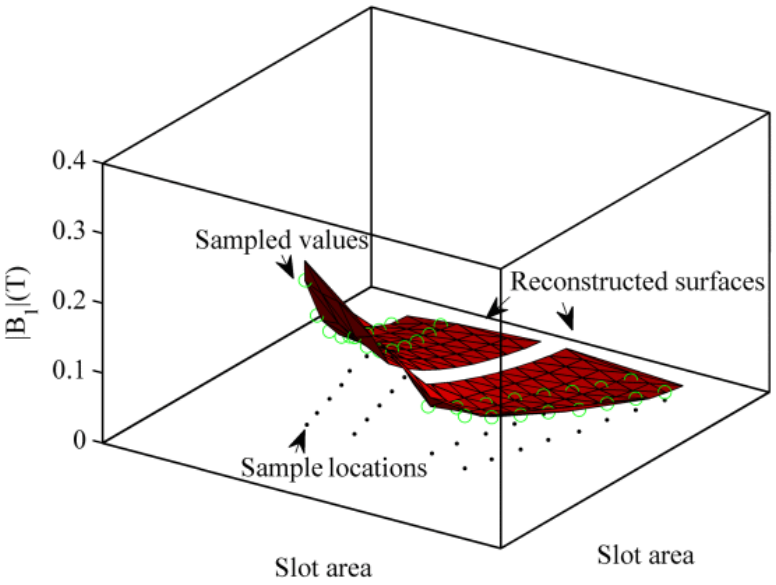

Fig. 6. Reconstruction of the field harmonics from the sample points using Delaunay triangulation method.

The maximum order of B harmonics that should be included in the loss analysis is design dependent. When the field values throughout the slot area are determined, using the prior information of the strand positions, the impinging field on each strand can be mapped. In Fig. 7, the mapped values of the impinging B over each strand are shown for the fundamental and the third harmonics. It can be seen once again that the magnitude of the slot leakage flux density monotonically increases for the strands that are closer to the air gap. The same trend exists for strands that are located toward the leading end of the rotor pole under motoring operation for CCW direction of rotation.

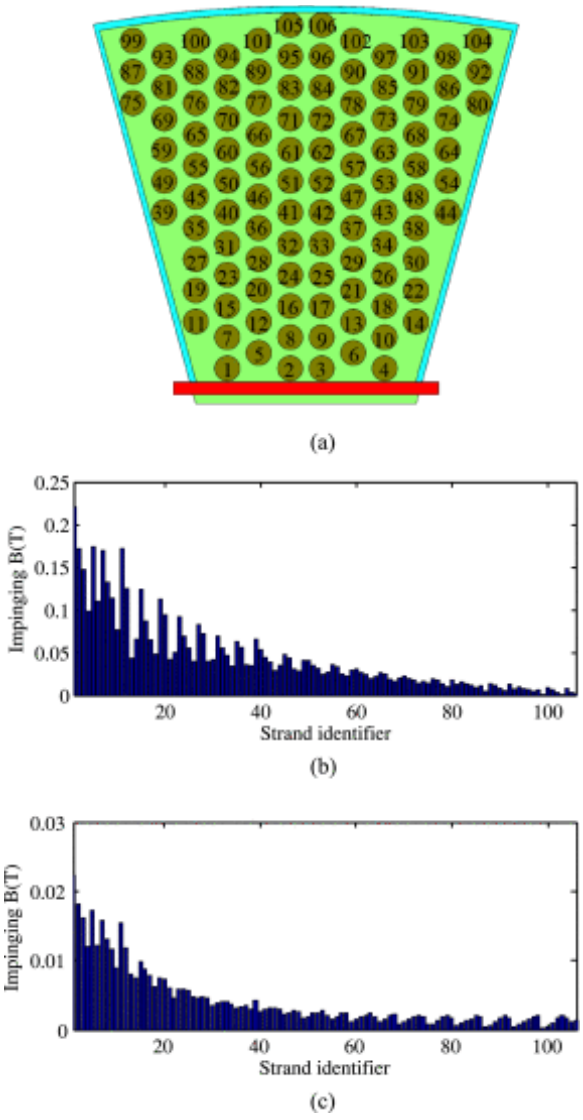

Fig. 7. Mapped flux on each individual strand. (a) Typical slot and strand numbers. (b) Fundamental component of the impinging B. (c) Third harmonic component of the impinging B.

E. Estimation of Value and Distribution of Eddy Current Losses

Upon derivation of the impinging $|B|$ on each strand, depending on the conductor shape, the loss models given in (2)–(5) can be used for estimation of strand eddy current losses in the conductors at the strand level. The resultant loss values using such an analysis on a typical slot are shown in Fig. 8(a)–(f) for a wide range of loading levels.

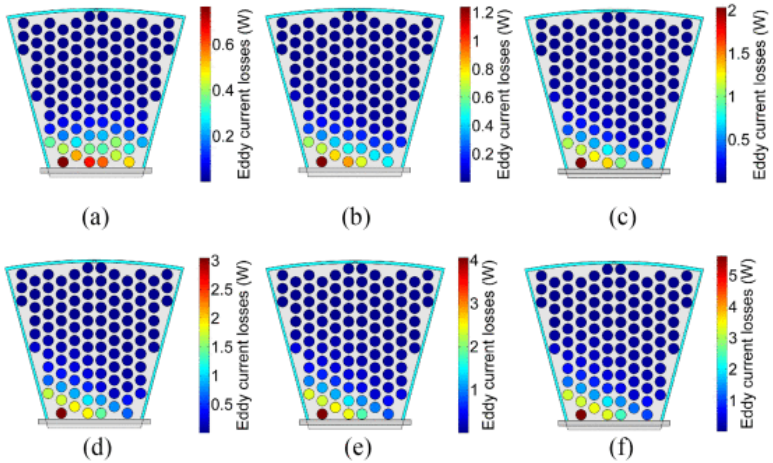

Fig. 8. Distribution of strand eddy current losses at different loading conditions. Note that the scales of the color-coded plots are different. (a) No load. (b) 25% load. (c) 50% load. (d) 75% load. (e) 100% load. (f) 125% load.

As can be seen in Fig. 8, using the developed method, in addition to the overall value of the eddy current losses, the distribution of such losses over each strand is obtained, which enables the incorporation of such losses into thermal analysis of the slot body that could be used in a coupled EM–thermal design optimization [2], [3].

SECTION IV. Case-Study Analysis and Experimental Verification on 12-Slot 10-Pole Machines

The method developed here was used for the calculation of eddy current losses in a 12-slot 10-pole interior permanent magnet (IPM) machine with V-type magnet layouts, as shown in Fig. 9(a). The all-teeth-wound stator winding consists of series coils each composed of 53 turns of AWG 12.5 wires, thus reducing to negligible levels the losses associated with circulating currents, which are essentially of a 3-D nature and cannot be accounted for by 2-D models such as the one presented here. The stator winding losses including the strand eddy current losses are calculated by the developed method and the results are compared with those obtained from a TS-FEA with detailed coil modeling, as shown in Fig. 9(b).

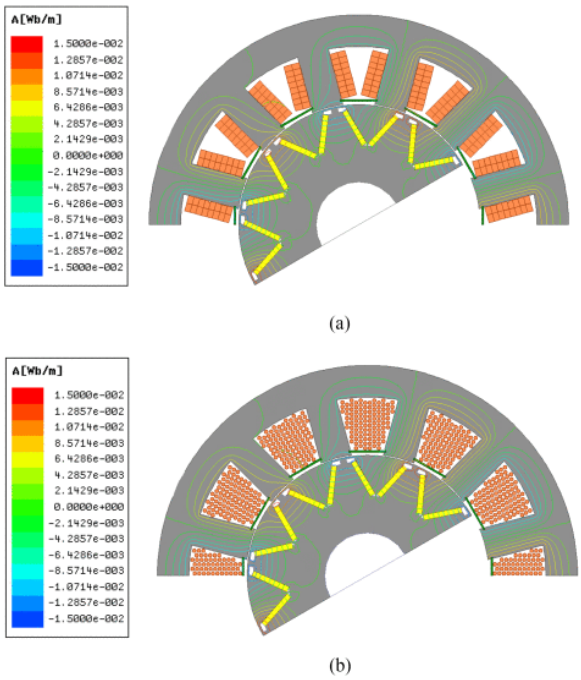

Fig. 9. Case-study investigation of a 10-hp generic industrial 12-slot 10-pole machine. (a) CE-FEA with flux mapping. (b) FEA with detailed coil modeling.

Three speeds of 1800, 6000, and 14 400 r/min, respectively, corresponding to excitation frequencies of 150 Hz, 500 Hz, and 1.2 kHz are considered in this study. Given the bare wire diameter d of 1.94056 mm, the skin depth δ of the copper conductors at the assumed operating temperature of 100 ◦C is 2.2 mm at the maximum frequency of 1.2 kHz, thus rendering insignificant the ac loss component due to the skin effect. Otherwise, (5) or simplified correction curves in engineering handbooks [1] can be used to account for skin effect losses.

Furthermore, since $d/\delta < 1$, the eddy current in the winding area could be assumed to be resistance limited, i.e., has negligible effect on the impinging field. This is illustrated in Fig. 10 for a given slot and rotor position of the case-study machine under the full-load condition. Fig. 10 compares the distributions of the flux density within the winding area, which are calculated using the proposed method and TS-FEA at the extremities of the excitation frequency. Slight differences could be attributed to the different meshing requirements between CE-FEA and TS-FEA. The field values along the slot peripheries and the current density distribution inside the conductors are also plotted in Figs. 11and 12, respectively. As could be seen in Figs. 10–12, although the current density distribution for the conductors closer to the slot top becomes non-uniform at higher frequencies, the calculated field density via CE-FEA still holds valid.

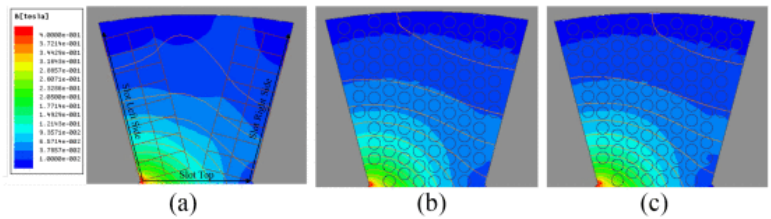

Fig. 10. Comparison of calculated field density within the slot area. (a) CE-FEA. (b) TS-FEA, 150 Hz. (c) TS-FEA, 1.2 kHz.

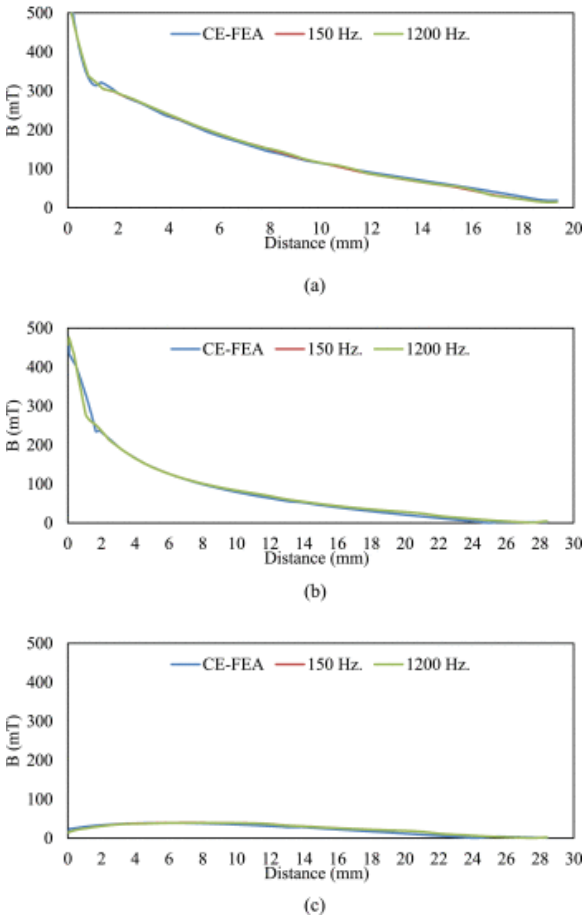

Fig. 11. Comparison of calculated field density along the slot peripheries. (a) Top of the slot (slot opening). (b) Left side of the slot. (c) Right side of the slot.

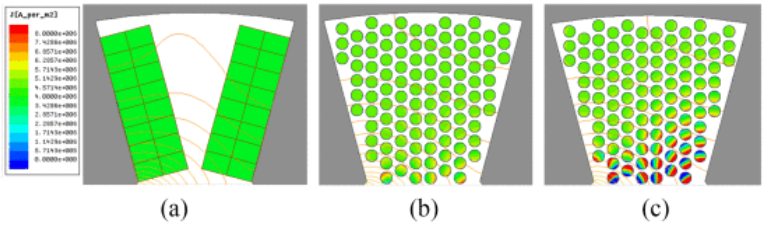

Fig. 12. Comparison of calculated current density within the slot area. (a) CE-FEA. (b) TS-FEA, 150 Hz. (c) TS-FEA, 1.2 kHz.

If $d/\delta > 1$, the effect of field variations on the eddy current losses could be accounted for by introducing a multiplier G_r to the losses calculated by (4) [1]

$$\begin{cases} G_r \approx 1 & d/\delta \Rightarrow 1 \\ G_r \approx \dfrac{32}{d^4/\delta}(d/\delta - 1) & d/\delta > 4 \\ G_r \approx (d/\delta)^{-}3 & d/\delta \Rightarrow \infty \end{cases}. \quad (7)$$

In light of the above discussions, the strand eddy current losses of the case-study machine are calculated over a wide range of motor loading conditions under maximum torque per ampere control for three different speeds at a winding temperature of 100 ◦C. The results obtained from the developed method and those from the TS-FEA

with detailed coil modeling are compared in Fig. 13(a)–(c). The required computation time is less than 80 s using the proposed method as opposed to 3370 s using the detailed FEA.

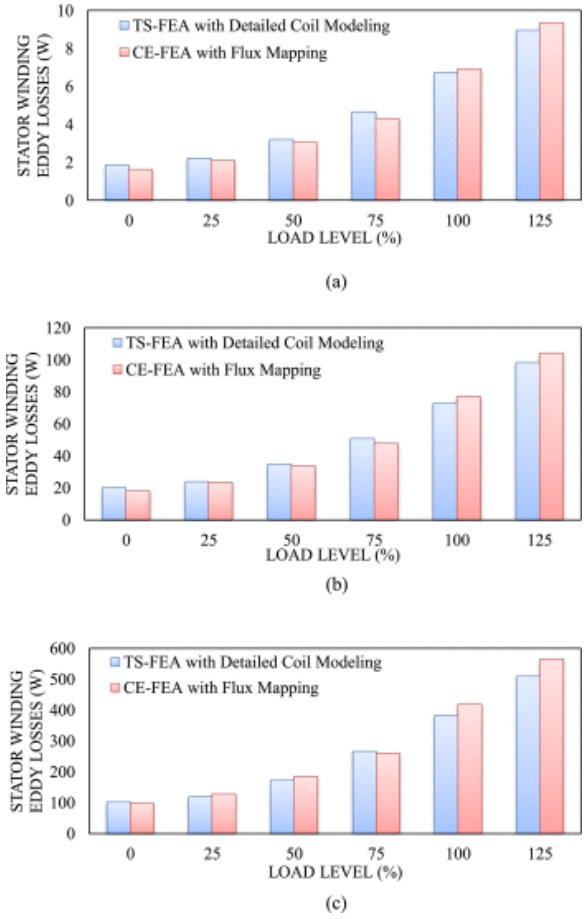

Fig. 13. Comparison of the accuracy of the loss calculation method over a wide range of frequencies and loading conditions. (a) 150 Hz. (b) 500 Hz. (c) 1200 Hz.

The estimation error of the proposed method when compared to the detailed TS-FE model is shown in Fig. 14 for several speeds and over a wide range of loading. The error is within a reasonable range given the computational efficiency of the proposed method.

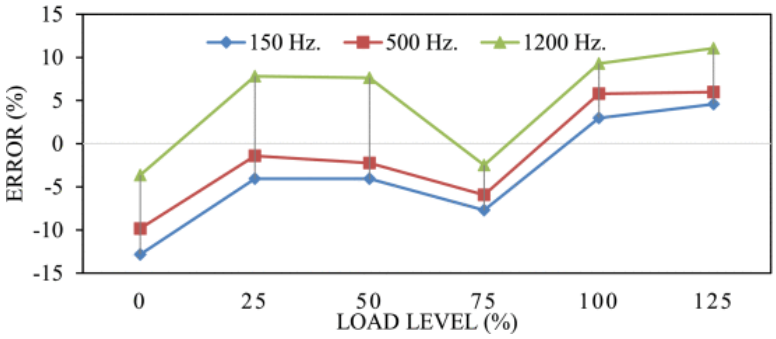

Fig. 14. Estimation error of the CE method of calculation of strand eddy current losses compared to the full-fledged TS-FEA with detailed coil modeling.

The variation of the ac to dc loss ratio $P_{\mathrm{ac}}/P_{\mathrm{dc}}$ due to the armature reaction under different loading levels is shown in Fig. 15. As can be seen in Fig. 15(a)–(c), strand eddy current losses constitute a larger contribution to the overall losses, $P_{\mathrm{ac}} = P_{\mathrm{dc}} + P_e$, under light load levels. The rate of increase of eddy current losses with respect to loading, which is mainly due to the elevated saturation level of the ferrous core and therefore increased leakage and fringing of flux into the slot area, is less than the rate of increase of dc copper losses P_{dc}, which is directly proportional to the current squared. This is especially true at lower frequencies as can be seen in Fig. 16. However, the eddy current losses are constantly present even at no-load conditions due to the presence of the time-varying field in the slots.

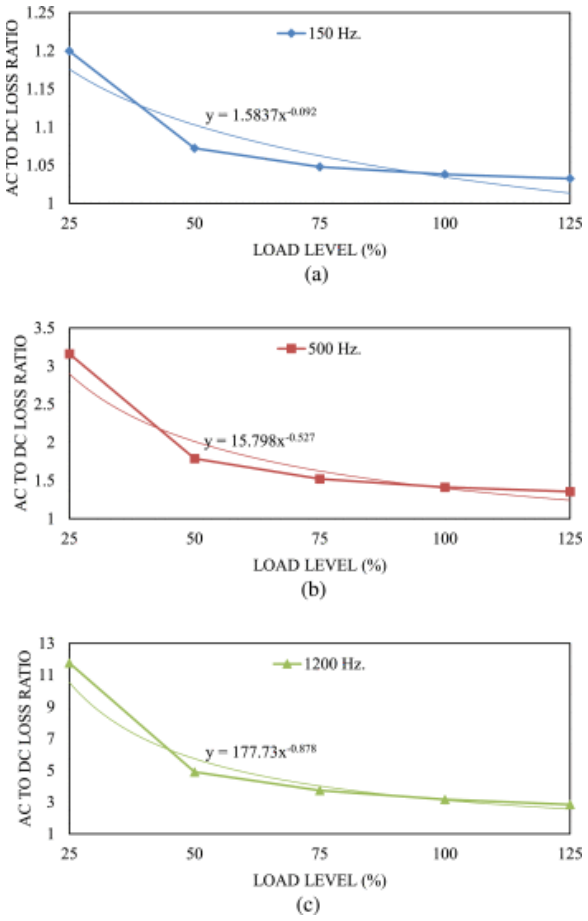

Fig. 15. Ratio of ac to dc losses over a wide range of loading conditions. (a) 150 Hz. (b) 500 Hz. (c) 1200 Hz.

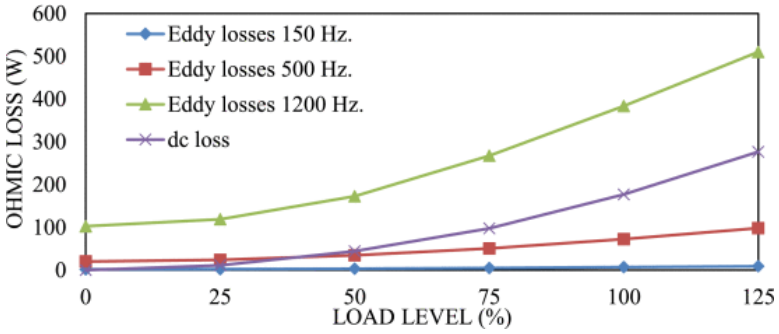

Fig. 16. Variation of dc ohmic losses and strand eddy current losses with respect to loading level.

The ratio of $R_{\mathrm{ac}}/R_{\mathrm{dc}}$, which is commonly used in the literature, is by definition not exposed to such large variations, and thus does not reflect them. Therefore, if the ratio of $R_{\mathrm{ac}}/R_{\mathrm{dc}}$ is to be used as a figure of merit

for comparison of ac losses between different design solutions, it should be derived and formulated under various loading conditions [33].

Here, for experimental demonstration of variation of $R_{\mathrm{ac}}/R_{\mathrm{dc}}$ with respect to frequency, and under one particular loading condition, the loss derivation method introduced in [19] is used. According to this method, several $R_{\mathrm{ac}}/R_{\mathrm{dc}}$ input data points are experimentally derived taking into account the end windings and bundle-level proximity effects, which cannot be accounted for by 2-D methods such as the one presented in this paper. The ac winding losses of a 12-slot 10-pole IPM machine were measured at different frequencies. The resultant $R_{\mathrm{ac}}/R_{\mathrm{dc}}$, which was obtained at 23 ◦C, is plotted in Fig. 17. The final winding power loss, including the effects of temperature, can be estimated using the following equation [19]:

$$P_{\mathrm{ac}|T} = P_{\mathrm{dc}|T_0}(1+\alpha(T-T_0)) + P_{\mathrm{dc}|T_0}\frac{\frac{R_{\mathrm{ac}}}{R_{\mathrm{dc}}}|_{T_0}-1}{(1+\alpha(T-T_0))^{\beta}} \tag{8}$$

where $P_{\mathrm{dc}|T_0} = 3R_{\mathrm{dc}}|_{T_0} I^2_{ph,\mathrm{rms}}$, α is the temperature coefficient of resistivity for copper conductors $\alpha = 3.93 \times 10^{-3} K^{-1}$, and $\beta < 1$ is an introduced factor that can be found by curve fitting (8) into the ac copper loss data for temperature T [19]. However, as shown through the analysis of the ac losses in the previous section, an additional curve fitting is required to account for an inclusive loss estimation at different loading conditions. This additional curve fitting is beyond the scope of this paper and will be investigated in a future work.

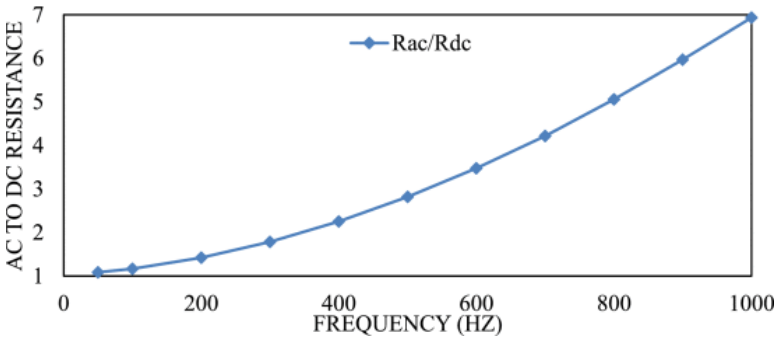

Fig. 17. Experimental demonstration of variation of $R_{\mathrm{ac}}/R_{\mathrm{dc}}$ for a 12-slot 10-pole machine at a winding temperature of 23 ◦C.

As mentioned previously, the presented ac loss calculation method yields both the overall eddy current ac losses due to the slot leakage and fringing flux, and also the distribution of such losses within the slot. The latter can be used for thermal analysis of the design candidates in a coupled EM–thermal optimization process [2], [3].

Here, to illustrate how the inclusion of the strand eddy current losses influences the temperature distribution within the slots, the thermal performance of the case-study motor in Fig. 9 is investigated. The thermal analysis is carried out in motor-CAD, which relies on fast lumped parameter thermal models suitable for coupled thermal–EM optimizations as presented in [2]. For this purpose, a typical liquid-based cooling system with stator water jackets is considered. The coolant is water with a flow rate of 10 L/min and an inlet temperature of 40 ◦C. Two scenarios are considered for this thermal analysis based on whether the strand eddy current losses calculated using the developed method are included, or only the dc ohmic losses are taken into account. The resultant average and maximum temperatures obtained for the full-load operation under three different speeds, corresponding to excitation frequencies of 150, 500, and 1200 Hz, are listed in Tables I and II. The large discrepancies in the temperatures obtained from the two scenarios based on whether or not the strand eddy current losses are included in the thermal analysis, especially as the speed and, thus, the frequency of operation increases, should be noted.

TABLE I. Winding Temperatures Based on DC Ohmic Losses Only

Speed	Max. Temperature	Ave. Temperature
1,800 r/min	75.8 °C	47.9 °C
6,000 r/min	84.0 °C	59.4 °C
14,000 r/min	129.7 °C	86.0 °C

TABLE II Winding Temperatures Including Stator Winding Strand Eddy Current Losses

Speed	Max. Temperature	Ave. Temperature
1,800 r/min	77.4 °C	65.3 °C
6,000 r/min	101.9 °C	85.2 °C
14,000 r/min	200.8 °C	162.4 °C

SECTION V. Conclusion

A method was developed for the calculation of strand eddy current losses in the stator windings of electric machines, which has the following characteristics:

1. it is FE based to take into account the complex geometry of the machine and the effects of saturation;
2. it is CE and suitable for integration into large-scale design optimization algorithms;
3. it is applicable to any variety of machines with different combinations of stator slots and rotor pole structures;
4. it estimates the maximum SF factor for each design candidate based on winding specs and slot geometry;
5. it estimates the value of eddy current losses due to slot leakage and fringing flux effects under any loading conditions, i.e., various torque and speed operating points;
6. it estimates the distribution of copper losses including the eddy current losses in the slots for rigorous thermal analysis of the stator windings.

The developed loss calculation method was implemented on an FSCW 12-slot 10-pole IPM machine with relatively large slot openings. The results over a wide range of loading conditions and operating frequencies were in good agreement with those obtained from a TS-FEA with detailed coil modeling. Meanwhile, the required computation time was significantly reduced using the presented method. The distribution of the losses in this case-study machine was used for a subsequent thermal performance analysis to underscore the importance of including strand eddy losses as a major loss component in high-speed machines, even if the stator winding conductors are stranded and transposed.

Using the developed loss calculation method, it was also shown that the variations of $P_{\mathrm{ac}}/P_{\mathrm{dc}}$ loss ratio with reference to the machine loading levels are not reflected in the common figure of merit represented by $R_{\mathrm{ac}}/R_{\mathrm{dc}}$ resistance ratio. Thus, if the $R_{\mathrm{ac}}/R_{\mathrm{dc}}$ ratio is to be used, additional treatment will be required to include the loading effects.

ACKNOWLEDGMENT

The authors gratefully acknowledge the software support of Motor Design Ltd., and ANSYS Inc.

REFERENCES

1. E. Snelling, Soft Ferrites: Properties and Applications, London, U.K.:Butterworths, 1988.

2. Y. Wang, D. Ionel, D. Staton, "Ultrafast steady-state multiphysics model for PM and synchronous reluctance machines", *IEEE Trans. Ind. Appl.*, vol. 51, no. 5, pp. 3639-3646, Sep./Oct. 2015.

3. W. Jiang, T. Jahns, "Coupled electromagnetic-thermal analysis of electric machines including transient operation based on finite element techniques", *Proc. IEEE Energy Convers. Congr. Expo.*, pp. 4356-4363, 2013.

4. M. Popescu, D. Dorrell, "Proximity losses in the windings of high speed brushless permanent magnet AC motors with single tooth windings and parallel paths", *IEEE Trans. Magn.*, vol. 49, no. 7, pp. 3913-3916, Jul. 2013.
5. L. Wu, Z. Zhu, D. Staton, M. Popescu, D. Hawkins, "Analytical model of eddy current loss in windings of permanent-magnet machines accounting for load", *IEEE Trans. Magn.*, vol. 48, no. 7, pp. 2138-2151, Jul. 2012.
6. P. Reddy, T. Jahns, T. Bohn, "Modeling and analysis of proximity losses in high-speed surface permanent magnet machines with concentrated windings", *Proc. Energy Convers. Congr. Expo.*, pp. 996-1003, 2010.
7. W. Zhang, T. Jahns, "Analytical 2-D slot model for predicting AC losses in bar-wound machine windings due to armature reaction", *Proc. IEEE Transp. Electrific. Conf. Expo.*, pp. 1-6, 2014.
8. A. Thomas, Z. Zhu, G. Jewell, "Proximity loss study in high speed flux-switching permanent magnet machine", *IEEE Trans. Magn.*, vol. 45, no. 10, pp. 4748-4751, Oct. 2009.
9. P. Reddy, Z. Zhu, S.-H. Han, T. Jahns, "Strand-level proximity losses in PM machines designed for high-speed operation", *Proc. 18th Int. Conf. Elect. Mach.*, pp. 1-6, 2008.
10. Y. Amara, P. Reghem, G. Barakat, "Analytical prediction of eddy-current loss in armature windings of permanent magnet brushless AC machines", *IEEE Trans. Magn.*, vol. 46, no. 8, pp. 3481-3484, Aug. 2010.
11. A. Bellara, H. Bali, R. Belfkira, Y. Amara, G. Barakat, "Analytical prediction of open-circuit eddy-current loss in series double excitation synchronous machines", *IEEE Trans. Magn.*, vol. 47, no. 9, pp. 2261-2268, Sep. 2011.
12. L. Wu, Z. Zhu, "Analytical investigation of open-circuit eddy current loss in windings of PM machines", *Proc. XXth Int. Conf. Elect. Mach.*, pp. 2759-2765, 2012.
13. N. A. Demerdash, H. Hamilton, "Effect of rotor asymmetry on field forms and eddy current losses in stator conductors due to radial flux", *IEEE Trans. Power App. Syst.*, vol. PAS-91, no. 5, pp. 1999-2010, Sep. 1972.
14. S. Iwasaki, R. Deodhar, Y. Liu, A. Pride, Z. Zhu, J. Bremner, "Influence of PWM on the proximity loss in permanent-magnet brushless AC machines", *IEEE Trans. Ind. Appl.*, vol. 45, no. 4, pp. 1359-1367, Jul./Aug. 2009.
15. A. Arkadan, R. Vyas, J. Vaidya, M. Shah, "Effect of toothless stator design and core and stator conductors eddy current losses in permanent magnet generators", *IEEE Trans. Energy Convers.*, vol. 7, no. 1, pp. 231-237, Mar. 1992.
16. R.-J. Wang, M. Kamper, "Calculation of eddy current loss in axial field permanent-magnet machine with coreless stator", *IEEE Trans. Energy Convers.*, vol. 19, no. 3, pp. 532-538, Sep. 2004.
17. P. Mellor, R. Wrobel, D. Salt, A. Griffo, "Experimental and analytical determination of proximity losses in a high-speed PM machine", *Proc. IEEE Energy Convers. Congr. Expo.*, pp. 3504-3511, 2013.
18. R. Wrobel, J. Goss, A. Mlot, P. Mellor, "Design considerations of a brushless open-slot radial-flux PM hub motor", *IEEE Trans. Ind. Appl.*, vol. 50, no. 3, pp. 1757-1767, May/Jun. 2014.
19. R. Wrobel, D. Salt, A. Griffo, N. Simpson, P. Mellor, "Derivation and scaling of AC copper loss in thermal modeling of electrical machines", *IEEE Trans. Ind. Electron.*, vol. 61, no. 8, pp. 4412-4420, Aug. 2014.
20. A. Fatemi, D. M. Ionel, N. A. O. Demerdash, D. A. Staton, R. Wrobel, Y. C. Chong, "A computationally efficient method for calculation of strand eddy current losses in electric machines", *Proc. IEEE Energy Convers. Congr. Expo.*, pp. 1-8, 2016.
21. P. Reddy, T. Jahns, T. Bohn, "Transposition effects on bundle proximity losses in high-speed PM machines", *Proc. IEEE Energy Convers. Congr. Expo.*, pp. 1919-1926, 2009.
22. M. van der Geest, H. Polinder, J. A. Ferreira, D. Zeilstra, "Current sharing analysis of parallel strands in low-voltage high-speed machines", *IEEE Trans. Ind. Electron.*, vol. 61, no. 6, pp. 3064-3070, Jun. 2014.
23. G. Y. Sizov, P. Zhang, D. M. Ionel, N. A. O. Demerdash, M. Rosu, "Automated multi-objective design optimization of PM AC machines using computationally efficient FEA and differential evolution", *IEEE Trans. Ind. Appl.*, vol. 49, no. 5, pp. 2086-2096, Sep./Oct. 2013.
24. A. Fatemi, N. A. O. Demerdash, T. W. Nehl, D. M. Ionel, "Large-scale design optimization of PM machines over a target operating cycle", *IEEE Trans. Ind. Appl.*, vol. 52, no. 5, pp. 3772-3782, Sep./Oct. 2016.

25. A. Fatemi, D. M. Ionel, M. Popescu, Y. C. Chong, N. A. O. Demerdash, "Design optimization of a high torque density spoke-type PM motor for a formula E race drive cycle", *IEEE Trans. Ind. Appl.*, vol. 54, no. 5, pp. 4343-4354, Sep./Oct. 2018.
26. Y. Wang, D. M. Ionel, M. Jiang, S. J. Stretz, "Establishing the relative merits of synchronous reluctance and PM-assisted technology through systematic design optimization", *IEEE Trans. Ind. Appl.*, vol. 52, no. 4, pp. 2971-2978, Jul./Aug. 2016.
27. A. Fatemi, D. M. Ionel, N. A. O. Demerdash, T. W. Nehl, "Fast multi-objective CMODE-type optimization of PM machines using multicore desktop computers", *IEEE Trans. Ind. Appl.*, vol. 52, no. 4, pp. 2941-2950, Jul./Aug. 2016.
28. P. Zhang, G. Y. Sizov, D. M. Ionel, N. A. O. Demerdash, "Establishing the relative merits of interior and spoke-type permanent-magnet machines with ferrite or NdFeB through systematic design optimization", *IEEE Trans. Ind. Appl.*, vol. 51, no. 4, pp. 2940-2948, Jul./Aug. 2015.
29. G. Carter, The Electromagnetic Field in Its Engineering Aspects, New York, NY, USA:American Elsevier, 1967.
30. G. Y. Sizov, D. M. Ionel, N. A. O. Demerdash, "Modeling and parametric design of permanent-magnet AC machines using computationally efficient finite-element analysis", *IEEE Trans. Ind. Electron.*, vol. 59, no. 6, pp. 2403-2413, Jun. 2012.
31. P. Zhang, G. Sizov, J. He, D. Ionel, N. Demerdash, "Calculation of magnet losses in concentrated-winding permanent-magnet synchronous machines using a computationally efficient finite-element method", *IEEE Trans. Ind. Appl.*, vol. 49, no. 6, pp. 2524-2532, Nov./Dec. 2013.
32. G. Y. Sizov, "Design synthesis and optimization of permanent magnet synchronous machines based on computationally-efficient finite element analysis", 2013.
33. R. Wrobel, A. Mlot, P. H. Mellor, "Contribution of end-winding proximity losses to temperature variation in electromagnetic devices", *IEEE Trans. Ind. Electron.*, vol. 59, no. 2, pp. 848-857, Feb. 2012.

Keywords

IEEE Keywords

Eddy currents , Conductors , Stator windings , Design optimization , Loss measurement , Analytical models , Computational modeling

INSPEC: Controlled Indexing

eddy current losses , eddy currents , finite element analysis , magnetic flux , magnetic leakage , optimisation , permanent magnet machines , stators , synchronous machines

INSPEC: Non-Controlled Indexing

fast finite element based method , stator windings , randomly wound electric machines , ac losses , constant slot fill factor , individual slot structure/dimensions , strand wire specifications , conductor strands , initial FE model , subsequent flux mapping technique , ac conductor losses , strand eddy current losses , electromagnetic machine behavior , thermal machine behavior , permanent magnet synchronous machine , higher slot leakage flux , slot opening fringing flux , loss effects , machine design , strand eddy current loss calculation

Author Keywords

AC copper loss , design optimization , eddy current loss , finite element (FE) method , high-speed permanent magnet (PM) machines , loss measurement